Application of Path Planning Algorithms to Robot Navigation in Radiation Plumes and Fields

Omololu Makinde[1], Shelly Bagchi[2], Christian H. Ramos[3], Christopher Wheatley[4]
[1] *Nuclear Disablement Team 2, 20th Chemical Biological Nuclear Radiological and Explosive Command*
Aberdeen Proving Grounds, MD 21005
omololu.o.makinde.mil@mail.mil
[2]*National Institute of Standards and Technology, U.S. Department of Commerce*
100 Bureau Drive, Gaithersburg, MD 20899
shelly.bagchi@nist.gov
[3]*University Of Maryland, College Park, MD 20742*
perseverancia@hotmail.com
[4]*University Of Maryland, College Park, MD 20742*
wheat1@terpmail.umd.edu

***Abstract*— The Armed Force of the United States Joint Publication 3-11 defines CBRN hazards as "CBRN materials that could create adverse effects if released or disseminated accidentally, deliberately, or even naturally". Critical to fighting in this environment is the ability to understand the CBRN joint operational environment and consider all hazards. A nuclear detonation would create such an environment. JP 3-11 instructs staff to conduct an awareness and understanding loop of activities that all surround identifying the source of the hazard and characterizing the operational environment. In order to accomplish this task after a nuclear detonation staff and responders will have to conduct a search in a radiological contaminated area. Similarly, nuclear power plants and facilities that work with highly radiated nuclear material have had accidents that lead to release of radioactive material confined inside a shielded building. Actions to remediate these kinds of accidents also begin with understanding the environment by searching through radiation fields. This article explores an outdoor and indoor scenario requiring searching through radiation fields and incorporates sampling-based path planning algorithms to generate the paths through the field. The article then offers approaches to use the generated paths as pre-mission planning tools to understand the effects of both the environment on robots/tools and the effect of introduction of robots, tools or humans into the environment.**

***Keywords*— Path planning, robotics, nuclear engineering, radiation plume, radiation isotope search, radiation field**

I. Introduction

The nuclear industry can be divided into four major fields of employment, namely, nuclear power, nuclear medicine, nuclear research and nuclear weapons. All components of these fields use facilities and fuel generated from the nuclear fuel cycle. Since the development of the first atomic weapon and execution of the Trinity Test, characterizing the radiation contamination field has been a scientific and operational challenge.

The reactor meltdown at Three Mile Island (TMI) was the first spur in robotic development in the nuclear field. At the time, the robotics industry was less than 20 years old, with little to no advances in computer vision, controls theory or planning, and with bulky hardware [1]. The accident led to an acceleration in research and development of robots for nuclear power plants. However, robots that could conduct autonomous or semi-autonomous tasks in dangerous environments were just being conceptualized.

The TMI accident led to four robots, namely SISI, Rosa, Rover and Fred, being employed extensively in remote surveillance, core defueling and decontamination [1]. However, TMI to Chernobyl to Fukushima nuclear incidents, there exists a common need to characterize the site conditions as soon as possible [2]. Research in the field is mostly focused on material and shielding solutions. However, software and algorithms can play a vital role.

This project takes the 2019 review of ground-based robotic systems for the characterization of nuclear environments [3] and demonstrates how the addition of search algorithms could help in planning and execution of radiation field characterization.

II. Related Work

Unlike most industries that use robots out of a desire to improve product quality or gain a competitive edge, the use of robots in the nuclear

industry is imperative due to reducing the human risks associated with working in radiation fields.

Hence there is a large body of work related to development of robots equipped with arms and cameras to move objects. Like robotic platforms developed for TMI clean-up [4]. Unmanned Aerial Vehicles are also being developed for radiation detection. These UAVs can map an area with low exposure received [5].

However, the shortfalls in the advancement in robotics for nuclear power plant accidents became evident in the aftermath of the Fukushima reactor accident in 2011 [3]. None of the technology developed could withstand the accumulated doses radiating from the core breach without significant cooling time. Major development efforts are underway for robots and radiation-hardened electronics that would solve this problem [2].

TABLE I
PARTIAL PERFORMANCE PARAMETERS OF RESPONSE ROBOTS FOR FUKUSHIMA DAIICHI ACCIDENT [2]

Robot model	Birthday	Institute	Size (W×L×H /mm)	Weight (kg)	Dose	Communication
FRIGO-MA	2012	Mitsubishi	490×650×750	38	10 Gy/h	Wired/Wireless
Survey Runner	2012	Topy	510×505×830	45	1000 Gy	Wired
Surface boat	2013	Hitachi	330×900×293	27	--	Wired
SC-ROV	2013	IRID	280×305×140	10	0.5 Gy/h Total 200 Gy	Wired
Rosemary	2013	IRID	500(W)×700(H)	65	--	Wireless
Raccoon	2013	ATOX	403×632×302	35	10 Gy/h	Wired
Arounder	2013	IRID	740×1200×1700	550	10 Gy/h	Wired
Kaniscrane	2014	Hitachi	700×2360×1430	1250	10 Gy/h	Wired
Gengo	2014	IRID	420×480×375	22	200 Gy	Wired
Trydiver	2014	IRID	480×628×378	40	200 Gy	Wired
Telesoopic	2014	IRID	509×440×826	70	1000 Gy	Wired/Wireless
Lake Fisher	2014	IRID	658×1038×1016	180	1000 Gy	Wired/Wireless
Sakura	2014	IRID	390(W)×500(H)	35	--	Wired/Wireless
MEISTeR	2014	IRID	700×1250×1300	550	100 Gy/h 1000 Gy	Wired
Smartphone	2015	TEPCO	77×319×105	0.787	1.3 Gy/h	Wireless
B1	2015	IRID	70×600×95	--	10 Gy/h 1000 Gy	Wired
Scorpion	2017	IRID	90×550×90	--	100 Gy/h Total 1000 Gy	Wired
PMORPH	2017	IRID	70×700×95	--	100 Gy/h Total 1000 Gy	Wired
DRV	2017	IRID	90×300×90	--	70 Gy/h	Wired
ROV	2017	IRID	130(D)×300	2	200 Gy	Wired

Table 1 shows the failure doses for robots developed for the Fukushima Daiichi accident [2]. None of these robots are capable of conducting area radiation characterization at radiation levels that would have been seen immediately after the accident, however, integrating path planning into the robot programming can help find the fastest path to characterizing an area and returning the robot prior to receiving a catastrophic total dose.

III. METHODS

A. *Radiation Field Modelling*

The Defence Land Fallout Interpretive Code (DELFIC) Fallout Planning Tool model a 1.2kt nuclear detonation in College Park Maryland. Figure 1 shows the plume from the model. application of path planning in a wide area radiation field.

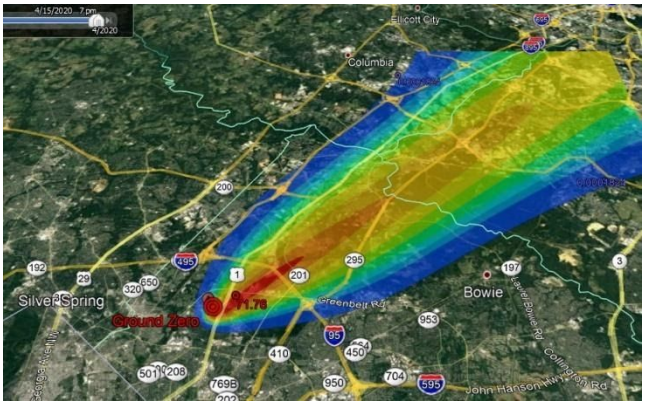

Figure 1. DELFIC plume for 1.2kt detonation at College Park, MD.

However, due to release restrictions, further details of the model can not be used for current analysis. Instead, a set of equations are used to model the exposure rate 24 hours after the incident. The detonation is modelled as a point isotropic source of caesium 137 radionuclide emitting 0.663 MeV gamma characteristic energy in dry air near sea level. Exposure as a function of distance, and obstacle are calculated with equations in Figure 2 and compared to values in Table 2.

TABLE 2
EXPOSURE RATES FROM DELFIC

Level (@R/h)	Cumulative Area (km^2)	Area (km^2)	Azimuth	Range (km)	Cell Count
30.0	0.2	0.2	154.2	0.3	97
10.0	0.7	0.5	106.5	0.6	198
3.0	2.4	1.7	104.8	1.0	680
1.0	6.8	4.4	95.3	1.8	1741
0.3	18.9	12.1	91.2	3.0	4826
0.1	48.1	29.2	90.8	4.6	11685
0.03	148.7	100.6	93.1	7.7	40251
0.01	442.1	293.4	94.5	12.8	117355
> 0	**	**	**	**	**

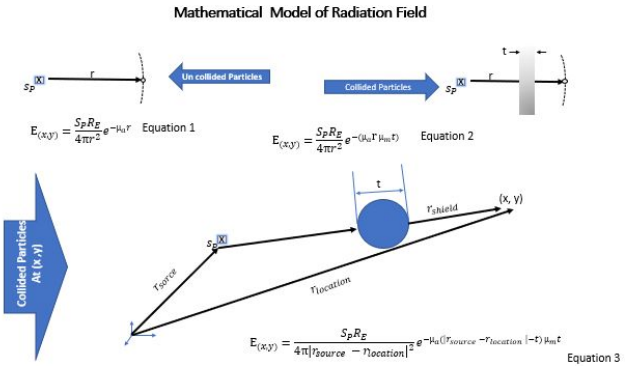

Figure 2: Exposure for Point isotropic source mathematical model (Faw 1996)

B. Sampling-Based Planning Algorithms

The methods implemented for this problem include two state-of-the-art sampling-based planning algorithms: Rapidly-Exploring Random Trees (RRT) and RRT*. RRT was developed in 2006 by LaValle as a motion planning algorithm which drives map exploration via movement towards randomly appearing nodes on the map. One notable feature of this method, which makes it useful for exploration within a radiation field, is the cost function. This cost function can be tailored based on heuristics that are specific to the problem of interest. For this topic, the primary metrics of concern are distance (from current node to random sample) as well as exposure rate on the map at the location of the current node. In this case, the distance already travelled (cost2come) is not of concern and thus is not incorporated into the RRT cost function. The driver for these modifications is due to the goal of obtaining a feasible path plan from start to goal, where shortest-distance is the primary factor until the robot enters a region of high radiation exposure, at which point shortest-distance becomes irrelevant and lowest-exposure paths become much more heavily favored.

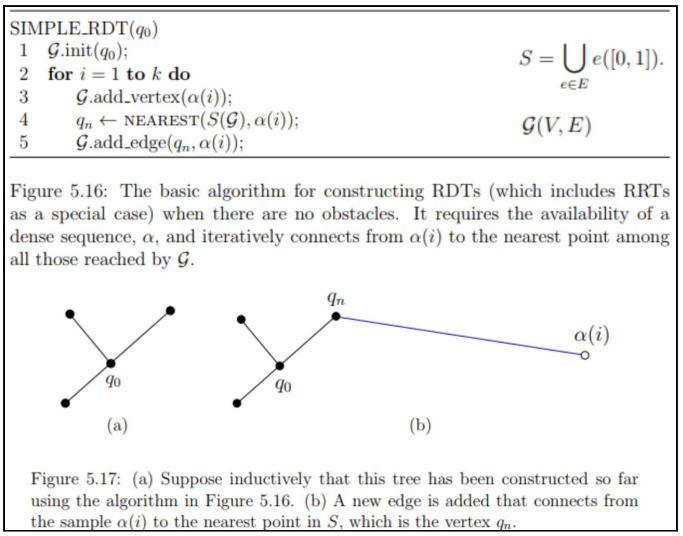

Figure 5.16: The basic algorithm for constructing RDTs (which includes RRTs as a special case) when there are no obstacles. It requires the availability of a dense sequence, α, and iteratively connects from $\alpha(i)$ to the nearest point among all those reached by $\mathcal{G}$.

Figure 5.17: (a) Suppose inductively that this tree has been constructed so far using the algorithm in Figure 5.16. (b) A new edge is added that connects from the sample $\alpha(i)$ to the nearest point in S, which is the vertex q_n.

Figure 3: Sample of RRT Algorithm Search Space.

Figure 3 shows a sample implementation of RRT. Note that RRT does not necessarily provide the optimal or 'best' solution. In this case, an "optimal" path is not the desired goal, in terms of shortest distance. The goal for RRT, as it applies to exploration of radioactive outdoor environments, is to obtain a feasible path plan which factors in both shortest-distance as well as exposure. Factoring in exposure, especially in notably high radioactive locations on the map, will cause exploration to venture in a way that is not always of shortest distance, but rather in such a way that attempts to circumvent/avoid regions of high exposure until a sufficiently high number of random samples forces the exampding RRT graph to continue exploring until the goal is reached.

RRT* was later developed by Karaman and Frazzoli as a variant of RRT which returns a probably optimal path (assuming one is available) [6]. The RRT* pseudocode can be seen in Figure 4. This paper applies advantages of RRT and RRT* to two separate scenarios.

Algorithm 4: Extend_{RRT^*}

$V' \leftarrow V$; $E' \leftarrow E$;
$x_{\text{nearest}} \leftarrow \texttt{Nearest}(G, x)$;
$x_{\text{new}} \leftarrow \texttt{Steer}(x_{\text{nearest}}, x)$;
if $\texttt{ObstacleFree}(x_{\text{nearest}}, x_{\text{new}})$ **then**
  $V' \leftarrow V' \cup \{x_{\text{new}}\}$;
  $x_{\min} \leftarrow x_{\text{nearest}}$;
  $X_{\text{near}} \leftarrow \texttt{Near}(G, x_{\text{new}}, |V|)$;
  for *all* $x_{\text{near}} \in X_{\text{near}}$ **do**
    if $\texttt{ObstacleFree}(x_{\text{near}}, x_{\text{new}})$ **then**
      $c' \leftarrow \texttt{Cost}(x_{\text{near}}) + c(\texttt{Line}(x_{\text{near}}, x_{\text{new}}))$;
      if $c' < \texttt{Cost}(x_{\text{new}})$ **then**
        $x_{\min} \leftarrow x_{\text{near}}$;
  $E' \leftarrow E' \cup \{(x_{\min}, x_{\text{new}})\}$;
  for *all* $x_{\text{near}} \in X_{\text{near}} \setminus \{x_{\min}\}$ **do**
    if $\texttt{ObstacleFree}(x_{\text{new}}, x_{\text{near}})$ *and* $\texttt{Cost}(x_{\text{near}}) > \texttt{Cost}(x_{\text{new}}) + c(\texttt{Line}(x_{\text{new}}, x_{\text{near}}))$ **then**
      $x_{\text{parent}} \leftarrow \texttt{Parent}(x_{\text{near}})$;
      $E' \leftarrow E' \setminus \{(x_{\text{parent}}, x_{\text{near}})\}$;
      $E' \leftarrow E' \cup \{(x_{\text{new}}, x_{\text{near}})\}$;
return $G' = (V', E')$

Figure 4: RRT* pseudocode [7].

IV. Methods

A. Scenario 1: Autonomous Search and Planning in an Outdoor Radiation Field

The goal of Scenario 1 is to demonstrate the use of a sampling-based search algorithm to provide a path with the least total accumulated exposure. The scenario is modelled to represent residual gamma radiation 24 hours after a 1.2 kt nuclear weapon detonation. It involves radiation fields in a wide outdoor area, surrounded by a field of debris. Within this environment is a radiation source that needs to be identified, characterized, and/or recovered.

The source used for mathematical calculation in this scenario is a Cesium-137 radionuclide emitting 9.5 x 10^{17} particles as an isotropic radiating point source in air. Particles move radially outward until interactions with debris which are shown as buildings and vehicles in Figure 5. The exposure at any point p is then calculated by:

$$\textit{Exposure Rate}\left(\frac{R}{hr}\right) = \frac{S_P R_x(E)}{4\pi|r_s - r_t|^2} e^{-\Sigma(\mu_i t_i)} \qquad \text{(Eq 1)}$$

where:

S_P = number of particles emitted at the source per unit time,

$R_x(E)$ = 1.835 x $10^{-8} E\left(\frac{\mu_{en}(E)}{\rho}\right)_{air}$ is the photon exposure response function for energy E = 0.662 MeV,

and $\frac{\mu_{en}(E)}{\rho}$ is the energy transfer coefficient in $\frac{cm^2}{g}$.

r_s and r_p are the coordinates of the source and point p in the map frame.

$\Sigma(\mu_i t_i)$ is the mass coefficient of an obstacle in the path of the source times the distance traveled through the obstacle.

Scenario 1 considers radioactive exposure as the primary driver for map exploration. Exposure is calculated at every point within the 450m x 232m map space (using 1-m grid resolution). This scenario assumes two obstacle types, buildings and vehicles. Buildings are assumed to be composed entirely of concrete and vehicles are assumed to be made of steel and chromium. The chromium components of the vehicles are modelled as an irradiation of chromium 50 to produce characteristic chromium 51 with 0.323 MeV gamma ray from neutron activation. Figure 5 shows a top-down view of the Scenario 1 map, a southern section of the University of Maryland (College Park) with pink polygons representing buildings (concrete obstacles) and green polygons representing vehicles (chromium-steel sources).

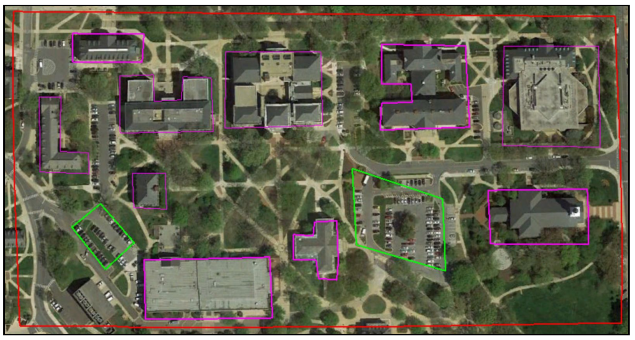

Figure 5: Google Earth aerial view of search area

In this scenario, the RICA robot in Figure 6 will be used to search the area in a simulated environment. RICA is a robot developed for radiation fields, and incorporates a sturdy metal body, tank-tread based differential drive for outdoor navigation, and gamma cameras (Ioannis Tsitsimpelis 2019). For this simulation it was assumed that the RICA robot could explore any terrain besides buildings and parking lots.

Figure 6: RICA Robot [3].

The robot will incorporate exposure rate with location data to search through the field using rapidly-exploring random trees (RRT). The RRT algorithm will find a path from a start point to a goal point by a constant evaluation of the nearest unexplored node. In this context, 'nearest node' indicates the existing node of lowest total cost. Each node *k* on the map is evaluated using the following total cost function:

$$\text{Total Cost}_k = w_1*(Cost2Go_k) + w_2*(Exposure\ Rate_k) \quad \text{(Eq 2)}$$

where:

Cost2Go=Euclidean distance from current node to random sample (m)

Exposure Rate (Eq 1) = Sum of the total radiation exposure rate at current node location (Roentgen/hr), influenced by the main source as well as surrounding obstacles

w_1, w_2 = Weights established via trial and error during algorithm implementation.

Figure 7 shows exposure rate in air represented as a homogeneous medium from the Cesium-137 point source. The source is located at the top right corner of the map, with the colour gradient from yellow to blue representing the isotropic radiation from the source.

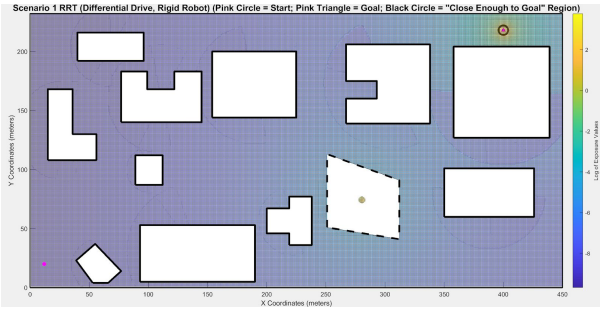

Figure 7: MATLAB model of search area with point source in homogeneous medium (air).

To simulate the operations of the RICA robot in this radiation field, the map space will be defined in MATLAB to provide exposure rates at each point on the map. The pre-computed rates will be supplied into the RRT algorithm as part of the cost in each node. An abstracted breakdown of the RRT search algorithm is outlined in the flowchart in Figure 8.

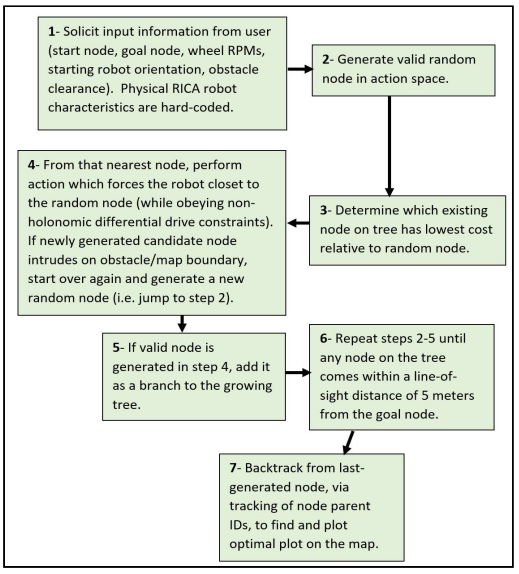

Figure 8: Rapidly-exploring random trees (RRT) algorithm flow chart.

B. Scenario 2: Optimal Path in Westinghouse Commercial Hot Cell

All nuclear processes that happen beyond a reactor require a hot cell. Hot cells are heavily shielded rooms with teleoperators positioned outside, around a special layer of lead-shielded glass. Workers bring articles into the cell via shielded ports, cranes, and manipulators. Vision in hot cells is often limited due to degradation in the glass panes over years of operation. Also, damage to the facility due to equipment malfunctions or natural disasters can render the teleoperation unusable. Recovery and hot cell clean-up is an extremely hazardous endeavour that consists of either manipulating large shielded partitions to get to the source in the room, or waiting years for acceptable radiation levels in the room.

Since there is prior knowledge of the environment in a hot cell, one can send a small robot into the room with a camera in the case of

loss of viewing capabilities in the windows. However, beyond a very short period, most cameras cannot withstand the high gamma radiation from spent fuel that is usually being processed in a hot cell; thus, the robot may not be functional by the time it reaches its goal, and also may not be retrievable. In this case, we intend to use Turtlebot 2 due to the small form factor and low cost to determine how far a robot can go inside the cell given an optimal path from a start to a goal point. This paper will use the RTT* algorithm to find the shortest navigable path to the source. The total exposure for this path is then calculated at each point to determine where the equipment failure will occur. Another application of the optimal path through the cell would be to determine the risk of criticality if a moderating element like a human moves along the path. This is useful because in situations where the radiation source is fissile or fissionable. Introduction of a moderated neutron could cause the environment to change from subcritical to critical thereby starting a chain reaction. Criticality calculation is an extremely specific and nuanced field of nuclear engineering that involves solving the diffusion transport equation for specific geometries. The key factors in any critical system is the geometry of all bodies, composition of fission radionuclide, and moderator. In a situation where a room composed of fissile material is currently not critical, a change into the environment by adding human beings would change the nuclear moderation and could lead to a critical configuration. Knowing the optimal path through such an area can allow for criticality calculations at each point on the path to determine the chance of criticality along that path. The hot cell under consideration is a Westinghouse commercial hot cell, shown in Figure 9.

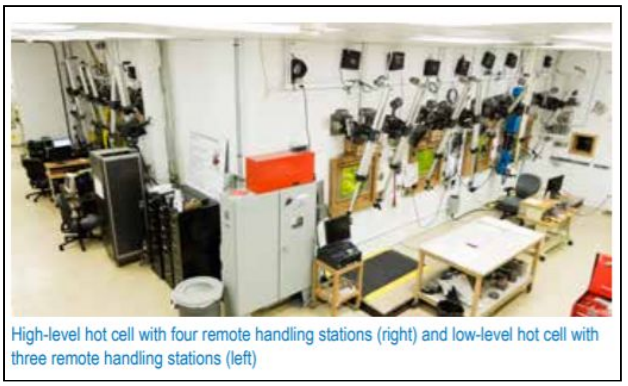

Figure 9: Outside a Westinghouse Commercial plant high-level cell

The hot cell is modelled in Python in an open configuration with three sources located next to respective shipping casks. Casks are modelled as lead shields. The cell is rated at 7000 $\frac{R}{hr}$, therefore the combined exposure rates from the sources is limited to this maximum. The equations in Figure 2 are used to calculate exposure rate at each point from all three sources, combined with shielding from each storage cask. Figure 10 shows the simulated room configuration plotted over a heat map of the sources' exposure rates in a homogeneous medium of argon. The lead-shielded casks are shown in white and a workbench is in purple.

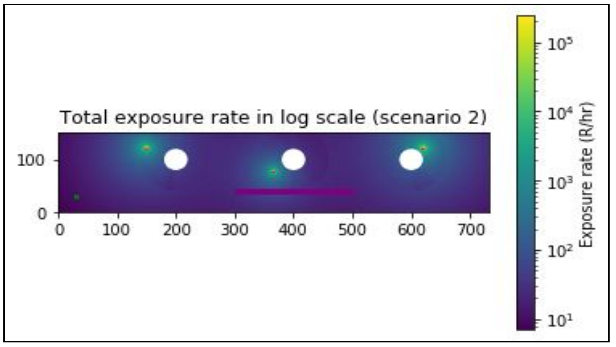

Figure 10: Hot cell objects shown over exposure rate heat map in Python.

The RRT* sampling method is used to search the cell. It utilizes a tree-based approach, which is summarized in the flow charts in Figure 11.

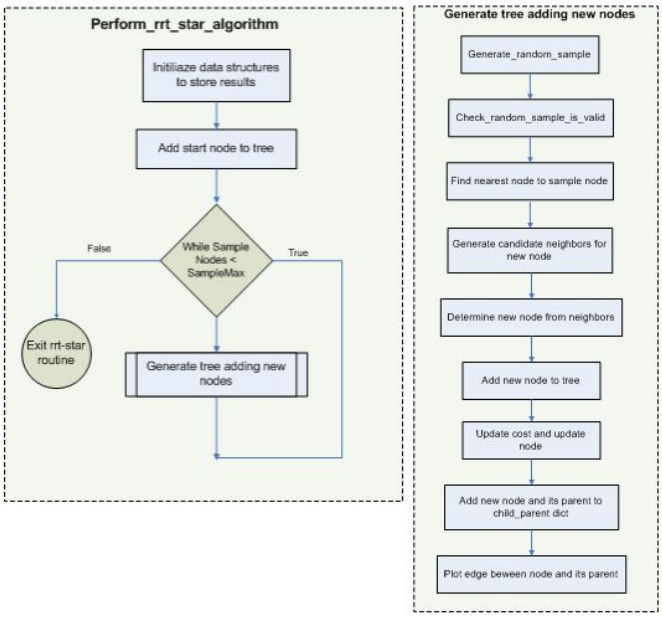

Figure 11: RRT* flow charts.

V. Robot and Environment Simulation

A. *Scenario 1: MATLAB and CoppeliaSim*

Scenario 1 implements the RRT algorithm, written in Matlab, and tested with a proof-of-concept 3D simulation in CoppeliaSim (previously known as V-REP, the Virtual Robot Experimentation Platform). For the simulation, buildings in the area are modelled as absorbing concrete polygons and shown in solid white. Cars are modelled as activated chromium polygons and shown in a grouping (e.g. parking lot area) with dashed borders. Hence, cars will add smaller, localized sources.

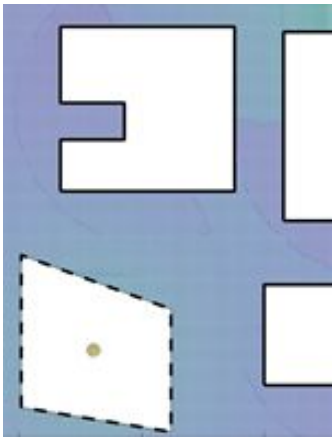

Figure 12: Concrete Obstacle Attenuations.

Figure 12 shows a close-up, top-down view of some of the concrete obstacles attenuating the radiation exposure. The attenuations are estimated as hemispheres in the opposite direction of the source to model how the buildings will provide some shielding, i.e. lower-exposure regions. Additionally, a lighter region can be seen around the diamond-shaped parking lot obstacle, which absorbs and re-emits a low amount of radiation, as opposed to the attenuating concrete. Vehicles within the parking lot are assumed to be composed of chromium metal.

The cost function from Eq. 2 is used for RRT sampling of the area. The weights were determined by trial and error after examining the simulated exposure values. The implemented weight for radiation exposure consideration (w_2) is 0.000001 and the implemented weight for distance consideration (w_1) is 0.999999. The result of this configuration leads to the RRT algorithm heavily favouring shortest-distance exploration in areas of low radiation exposure, relative to the source strength, and heavily favouring lowest-exposure exploration in areas of high exposure. This is the ideal approach since the RICA robot is not notably sensitive to radiation exposure across the map, except for areas nearby the goal source.

Scenario 1 is modeled assuming differential drive constraints, meaning each wheel can drive with individual RPMs. For example, if the user inputs RPMs of [5,10] at the start of the simulation, then the following wheel speed configurations are available for performing RRT (for [Left Wheel RPM, Right Wheel RPM]): [0,0], [0,5], [5,0], [5,5], [5,10], [10,10], [0,10], [10,5].

From experimentation, it was determined that RRT exploration becomes infeasible if RPMs greater than 8 RPM are used. This is because, given the small dimensions and wheel separation of the RICA robot, the robot will tend to move in circular loops if sufficiently high RPMs are being implemented. Maximum wheel RPMs of 8 are assumed for the remainder of this analysis, as it allows for freedom to explore the map, but also yields a feasible/realistic path plan without recursive looping. Figure 13 compares how the

exploration tree expands with different RPM assumptions. Note that RPMs even as high as 12 result in recursive looping, and RPMs of no greater than 8 allow for the freedom to perform useful/feasible actions without moving backwards.

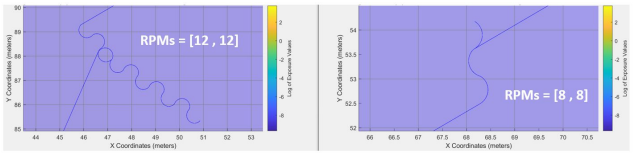

Figure 13: Tree Expansion Result for Different RPMs.

B. Scenario 2: Python and ROS-Gazebo

Scenario 2 implements the hot cell map in Python 3.7, with a 3D simulation in ROS-Gazebo. The 2D simulated environment is shown in Figure 10, with the heat map of exposure visualized in log-scale, with shielding from lead casks and workbench in the room.

The RRT* algorithm was utilized for this scenario as previously mentioned. The cost function used was the sum, *cost = cost2come + cost2go*. This provides the room operators the fastest path from one point in the hot cell to any other point. This simulates a situation where the actual exposures are known by the planner, and the exposure limit for a camera or another tool is known. By summing exposures along the optimal path the planner knows when and where the camera or tool will most likely malfunction.

Another instance where the optimal path could be applied in hot cells, is the prediction of criticality. If the source in the cell was a fissile material like some isotopes of Uranium and Plutonium, the optimal path generated by RRT* then represents the path to move material through the space with the least amount of change to the environment configuration. Using codes that solve the diffusion transport equation, planners can check each position to determine "k effective" (measure of criticality of a system) when an object is in that position.

The number of samples, a user-determined parameter for RRT*, allows tuning of the algorithm for a tradeoff between runtime and accuracy / optimality [9]. From experimentation, 700 samples were used to provide a sufficiently direct path.

The Turtlebot 2 was represented in the non-holonomic environment by utilizing Dubins Curves [10]. The Dubin Car approach consists of modeling the robot as a car that can only move forward within non-holonomic constraints [11]. Therefore, Dubin Curves make use of a maximum turning rate to determine the minimum turning radius the robot travels as a path is generated from one node to the next. Dubin Curves are based on geometric analyses and use three basic moves, Left (L), Right(R) and Straight(S), to generate the following six combinations of movements: (LSL , RSR, RSL, LSR, RLR, and LRL). These motions are considered when implementing the RRT* algorithm for this scenario[1] [12].

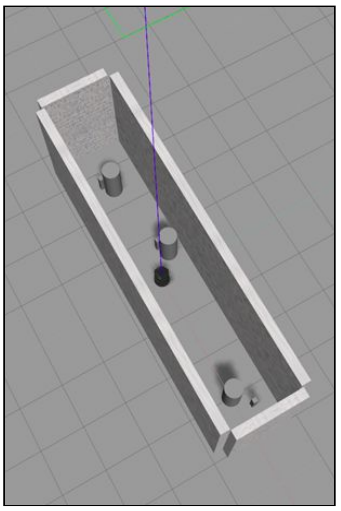

Figure 14: Scenario 2 world built in Gazebo.

Figure 14 shows the representation of the world built in ROS-Gazebo. The Turtlebot 2 can be seen in the center of the scene.

The node graph for this simulation is shown in Figure 15. The controller uses the odom topic to subscribe to the position of the robot via the nav_msgs message type. It receives the odometry message of coordinates of the robot. The node then publishes positions along the generated path at a constant velocity using the euler_from _quaternion transformation to convert the angles from odometry orientations. The next set of positions are published

[1] Andrew Walker's implementation was utilized: https://github.com/AndrewWalker/Dubins-Curves

via “cmd_vel_mux/input/navi” topic to the turtle bot’s base.

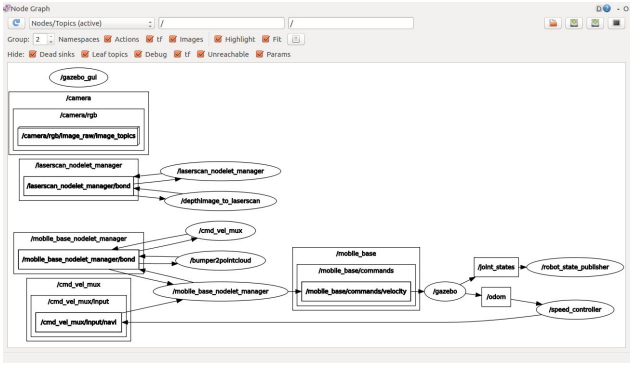

Figure 15: ROS node graph.

VI. Results

A. *Scenario 1 Results*

A sample RRT result can be seen in Figure 16, along with the exploration graph/tree. Note that, per the weights assigned within the cost function, that the path tends to prefer exploration within the attenuation regions created by the concrete obstacles (i.e. the hemispherical regions adjacent to each building obstacle). However, exploration becomes much more evasive as the exploration graph approaches the radiation source. This is by design such that the robot becomes much more careful while exploring around the source, and considers areas of low exposure rather than exploring the shortest distance in the direction of random samples.

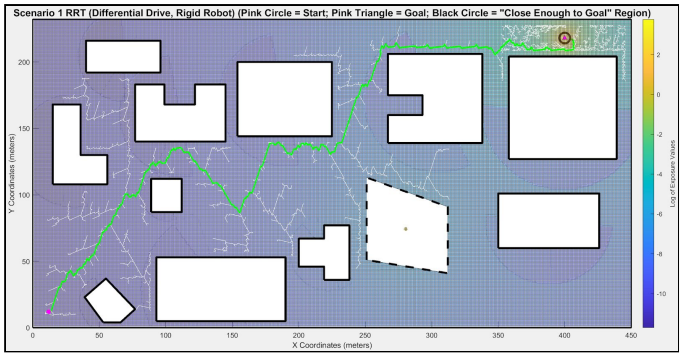

Figure 16: Scenario 1 RRT Exploration and Final Path Example.

The final path is then projected onto the real-world map similar to Figures 5 and 18. RRT is nondeterministic, therefore it does not guarantee the same path over multiple runs. Multiple runs are needed to find the lowest-exposure path option.

Figure 17 below shows a trace of the same RRT motion planning example except in a VREP simulation environment. All obstacles were derived and constructed from primitive 3D shapes such as cuboids. A 3D model of the RICA robot was not readily available at the time of this analysis, so a Pioneer P3DX robot was used instead due to its similar dimensionality to the RICA robot.

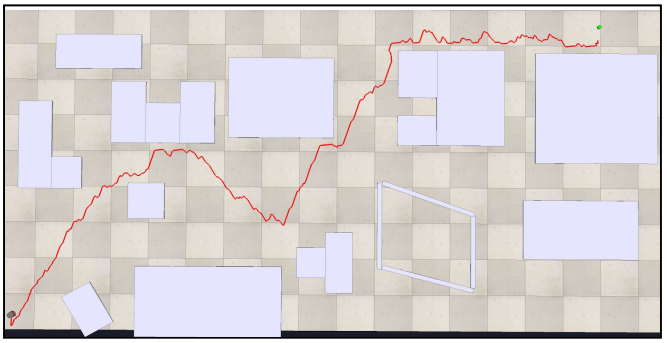

Figure 17: Scenario 1 RRT Exploration and Final Path Example.

Since RRT is a non-deterministic motion planning method, a post-analysis of multiple resulting paths is needed when devising a feasible plan. Figure 18 illustrates the best path for five separate simulation iterations where the robot starts in the bottom-right corner of the map, and where the goal source is in the top-left corner of the map. The differential drive parameters do not exceed 8 RPM for any of these simulations.

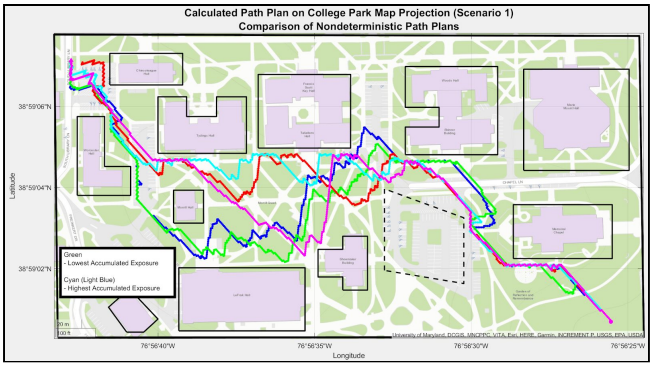

Figure 18: Visualization of 5 Non-Deterministic Path Plans for Differential Drive RRT (on Latitude/Longitude MATLAB Projection).

The most feasible plan in this case would be the green path, since it possesses the lowest accumulated radiation exposure throughout its transit. Visually this makes sense given the green path maintains the greatest clearance from the parking lot obstacle and given that it approaches the source from the south, shielding itself behind

obstacles until arriving at the source. The cyan line possesses the highest accumulated radiation exposure, which makes sense given that it approaches the source in a 'zig-zag' motion. This behavior illustrates how the algorithm attempted to circumvent exploration near the source, but actually resulted in the robot exploring the highest-exposure area for a longer duration of time. Table 3 shows the list of accumulated exposure rates (in R/hr) for each of the five non-deterministic path plans that were assessed for differential-drive RRT.

TABLE 3
EXPOSURE RATE RESULTS FROM 5 RUNS OF RRT

Path Option	Total Accumulated Exposure (R/hr)
Green	3.4330e9
Blue	3.4788e9
Cyan	6.8317e9
Red	5.1594e9
Magenta	5.3008e9

In a real-world implementation, a feasible path plan would be determined by evaluating many, many more path planning results. From these plans, the mean and standard deviation of total exposure rate can be calculated in the covariance matrix. This analysis would be useful in approximating the lower and upper limits on exposure in the situation, and determining whether the robot or human can be safely sent in.

B. Scenario 2 Results

A performance comparison was done for RRT vs RRT* to justify use of the heavier algorithm. Table 4 shows the total distance of paths achieved from each algorithm (with only one run of RRT), while Table 5 shows the runtime of the same test runs.

TABLE 4
TOTAL PATH DISTANCE FOR RRT VS RRT*

TEST POINTS	RRT	RRT*
Point Test 1 (110,110)	434.2 cm	120 cm
Point Test 2 (325,125)	1076 cm	454.1 cm
Point Test 3 (650,75)	1664 cm	1043.7 cm

TABLE 5
ALGORITHM RUNTIME FOR RRT VS RRT*

TEST POINTS	RRT	RRT* (700 samples)
Point Test 1 (110,110)	4 sec	142.3 min
Point Test 2 (325,125)	145 sec	143.3 min
Point Test 3 (650,75)	160 sec	121.3 min

As expected, RRT* yields a much shorter-distance path, but takes significantly longer to compute. This is acceptable in the hot cell scenario since the map is available ahead of time and the use is for post computational analysis of effects of the environment on equipment using the path, or the effect of moderators on the path.

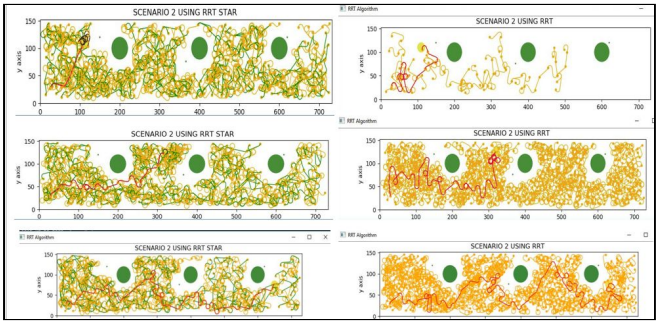

Figure 19: Visualization of RRT and RRT* exploration in the hot cell.

Figure 19 shows the resulting exploration from the comparative tests, with RRT* on the left and RRT on the right. The RRT* paths can be seen to be more direct and contain less loops. However, both results would need to be smoothed and optimized for practical usage.

VII. CONCLUSIONS & FUTURE WORK

The outcomes from Scenario 1 show that path planning can provide several useful outcomes in the case of a radiation detonation event. As demonstrated, a robot could be tasked to find the radiation source and create a rudimentary map of

the exposure in the area. The robot could additionally be tasked to find a specific location in the area, potentially for search-and-rescue or retrieval of important or dangerous items. Finally, the resulting path can be useful for humans to enter the radiation area while limiting their exposure to a safe level if possible.

Scenario 2 provides a solution for radiation finding an optimal path through an indoor radiation field by using the path generated to determine the effects of exposure on items traveling through the path It also provides the criticality engineer a tool to use to determine effects of items moving through a subcritical nuclear system. The extreme exposure in this situation and difficulty of teleoperation makes autonomous navigation a necessity. Although the levels of exposure may result in failure of the robotic system, a partial plan can be achieved and picked up later on by a second mobile platform. Some hot cells, including the Westinghouse cell discussed above, also include equipment such as industrial robot arms. These could potentially be used to swap parts on the robot model as they fail.

As future work, Scenario 1 can be improved through implementation of a path-correction or optimization algorithm (such as RRT* or RRT SMART). The fidelity of the Scenario 1 model can be improved as well, namely in regards to defining the radiation/exposure field across the map. Currently, attenuation regions exist as semicircles, located 180 degrees opposite the direction of goal/source. These regions represent areas of the map that are shielded from source radiation. In reality, these regions exist more so as conic sections that trail off as they move farther away from the source. In the future, the fidelity of this model can be improved by implementing these more accurate geometries. Another improvement to the model would be to utilize the DELFIC tool for more accurate exposure readings.

In future work, Scenario 2 would be modified to consider the particle transport equations using Monte Carlo. This would implement the more accurate stochastic versions of the exposure formulas, rather than the deterministic approximations used for simplicity in these simulations. Further, criticality predictions could be incorporated into the planning algorithm. This would allow us to determine whether a human can potentially move through the cell without causing a nuclear chain reaction. Finally, simulating the swap of robots and/or parts in the hot cell can provide a more accurate representation of the whole scenario.

Acknowledgment

The authors wish to acknowledge Lieutenant Colonel Scott Key, Lieutenant Colonel Brett Carrey, and Mr. Clem Gains for review and advice on the project.

References

[1] Moore, T. (1985). Robots for nuclear power plants. IAEA Bulleting, Nuclear Power and Electronics, 31-39.

[2] Qihao Zhanga, W. Z. (2018). Research Progress of Nuclear Emergency Response Robot. IOP Conf. Series: Materials Science and Engineering (p. 452). Mianyang 621700,: IMMAEE.

[3] Ioannis Tsitsimpelis, C. J. (2019). A review of ground-based robotic systems for the characterization of nuclear. Progress in Nuclear Energy, 109-124.

[4] TMI-2 Remote Cameras, Teleoperators and Other Potential Nuclear Applications. (1987, July to September). Nuclear Safety, 28.

[5] Nicholas Tsoulfanidis, S. L. (2011). Measurement and Detection of Radiation. Boca Raton, FL: CRC Press, Taylor & Francis Group.

[6] Karaman, S., & Frazzoli, E. (2010). Incremental sampling-based algorithms for optimal motion planning. Robotics Science and Systems VI, 104(2).

[7] LaValle, S. M. Planning Algorithms, 2006

[8] Joint Publication 3-11: Operations in Chemical, Biological, Radiological, and Nuclear Environments, 29 October 2018

[9] Walker, A. (2011). "Hard Real-Time Motion Planning for Autonomous Vehicles", PhD thesis, Swinburne University.

[10] Dubins, L.E. (July 1957). "On Curves of Minimal Length with a Constraint on Average Curvature, and with Prescribed Initial and Terminal Positions and Tangents". American Journal of Mathematics 79 (3): 497–516

[11] Shkel, A. M. and Lumelsky, V. (2001). "Classification of the Dubins set". Robotics and Autonomous Systems 34 (2001) 179–202

[12] Walker, A. (2008--) Dubins-Curves: An open implementation of shortest paths for the forward only car. https://github.com/AndrewWalker/Dubins-Curves